Host-directed FDA-approved drugs with antiviral activity against SARS-CoV-2 identified by hierarchical *in silico/in vitro* screening methods

Tiziana Ginex,[1, §] Urtzi Garaigorta,[2, §] David Ramírez,[3] Victoria Castro,[2] Vanesa Nozal,[1] Ines Maestro,[1] Javier García-Cárceles,[1] Nuria E. Campillo,[1] Ana Martinez,[1] Pablo Gastaminza,[2,*] Carmen Gil[1,*]

[1]Centro de Investigaciones Biológicas Margarita Salas-CSIC, Ramiro de Maeztu 9, 28040 Madrid (Spain)

[2]Centro Nacional de Biotecnologia-CSIC, Calle Darwin 3, 28049 Madrid (Spain)

[3]Instituto de Ciencias Biomédicas, Universidad Autónoma de Chile, Llano Subercaseaux 2801 – piso 6, Santiago, Chile.

[§]Both authors contribute equally to this work

Abstract

The unprecedent situation generated by the COVID-19 global emergency has prompted scientists around the world to actively work to fight against this pandemic. In this sense, it is remarkable the number of drug repurposing efforts trying to shed light into the COVID-19 patients' treatment.

In the attempt to proceed toward a proper rationalization of the search for new antivirals among approved drugs, we carried out a hierarchical *in silico/in vitro* protocol which successfully combines virtual and biological screening to speed up the identification of host-directed therapies against COVID-19 in an effective way.

A successful combination of a multi-target virtual screening approach focused on host-based targets related to viral entry and experimental evaluation of the antiviral activity of selected compounds has been carried out. As a result, three different potentially repurposable drugs interfering with viral entry, cepharantine, imatinib and efloxate, have been identified.

Keywords: SARS-CoV-2 evaluation, COVID-19, drug repurposing, host-based targets, virtual screening, entry inhibitors

INTRODUCTION

Together with severe acute respiratory syndrome coronavirus (SARS-CoV) and Middle East respiratory syndrome coronavirus (MERS-CoV), SARS-CoV-2 is the third pathogenic and transmissible coronavirus emerged in humans. This new coronavirus (CoV) is the causative agent of the present pandemic of coronavirus disease named COVID-19 first reported in Wuhan (China) (1). Since there is no effective treatment available and given the urgency of the pandemic, the repurposing of approved drugs is the only alternative to find a cure for the present emergency. In fact, several clinical trials are currently ongoing to prove the efficacy of old drugs in COVID-19 patients (2). Such is the case of the drugs including in the SOLIDARITY clinical trial (remdesivir, hydroxychloroquine, lopinavir/ritonavir and interferon-beta1a), launched by the WHO in dozens of countries that showed little or no effects on hospitalized COVID-19 patients at proposed dose regimens (3). Moreover, the only drug approved by the FDA for the treatment of extreme-ill patients is remdesivir (4), an antiviral originally developed for Ebola virus infection (5).

Although in principle not very innovative, drug repurposing is a promising approach to accelerate the drug discovery process which allows to increase the productivity of the pharmaceutical companies (6), and fill the gap existing in unmet diseases such as rare or infectious diseases (7, 8). In viral infections lacking of an effective treatment, drug repurposing combined with drug validation in animal models has enhanced the number of potential antivirals with known mechanism of action (9).

The COVID-19 global emergency has generated an unprecedented situation, which prompted scientists all around the world to actively work in all imaginable aspects related to SARS-CoV-2. In only few months, the knowledge of SARS-CoV-2 significantly increased and the available information today is quite large. Together with the efforts to better understand the epidemiology, virus structure and life cycle, several therapeutic targets to guide the drug discovery research have also emerged (10). In this regard, it is remarkable the number of drug repurposing efforts trying to shed light into the COVID-19 patients treatment (11, 12). Today, far from initial opportunistic and mainly serendipitous discoveries in the drug repurposing field, a number of candidates have been proposed to be repurposed for COVID-19 based on different *in silico* and *in vitro* studies (13).

In the attempt to proceed toward a proper rationalization of the search for new antivirals among approved drugs, we here implement a hierarchical *in silico/in vitro* protocol, which successfully combines virtual and biological screening to speed up the identification of anti-SARS-CoV-2 agents in an effective way.

Moreover, as viral mutations represent one of the main challenges to overcome with antiviral therapies, we carried out a multi-target virtual screening protocol focused on druggable targets related to viral entry followed by biological screening against SARS-CoV-2 to identify host-directed therapies against COVID-19. In this regard, eight proteins mainly involved in SARS-CoV-2 entry and trafficking were considered.

The US Drug Collection of 1789 compounds of FDA approved drugs was screened toward these targets, which consisted on the proteases TMPRSS2, Furin and Cathepsin L, the kinases AAK1, GAK and PIKfyve as well as the two-pore ion channel TPC2. Additionally, the receptor binding domain (S-RBD) of the viral Spike (S) glycoprotein, which is recognized by the host protein, ACE2 during virus attachment, was included in the analysis. A total of 173 FDA repurposable drugs were selected from virtual screening and subsequently experimentally evaluated. Primary hits were validated using several methods involving viral antigen detection as well as viral RNA load in infected cells. Confirmed candidates were subsequently tested for their ability to interfere selectively with viral entry in a surrogate model of infection. This process led to the identification of cepharantine, imatinib and efloxate as selective SARS-CoV-2 entry inhibitors, together with a panel of non-selective entry inhibitors that could be considered for drug repurposing.

RESULTS

Virtual screening against selected targets

A hierarchical virtual screening (VS) approach was applied on crucial SARS-CoV-2 protein targets in the attempt to find repurposable agents from the original list of FDA approved drugs. Among all the proposed druggable targets for SARS-CoV-2, eight proteins responsible for virus entry and trafficking were selected in this study. A schematic representation of their role in virus entry and trafficking is displayed in **Figure 1**.

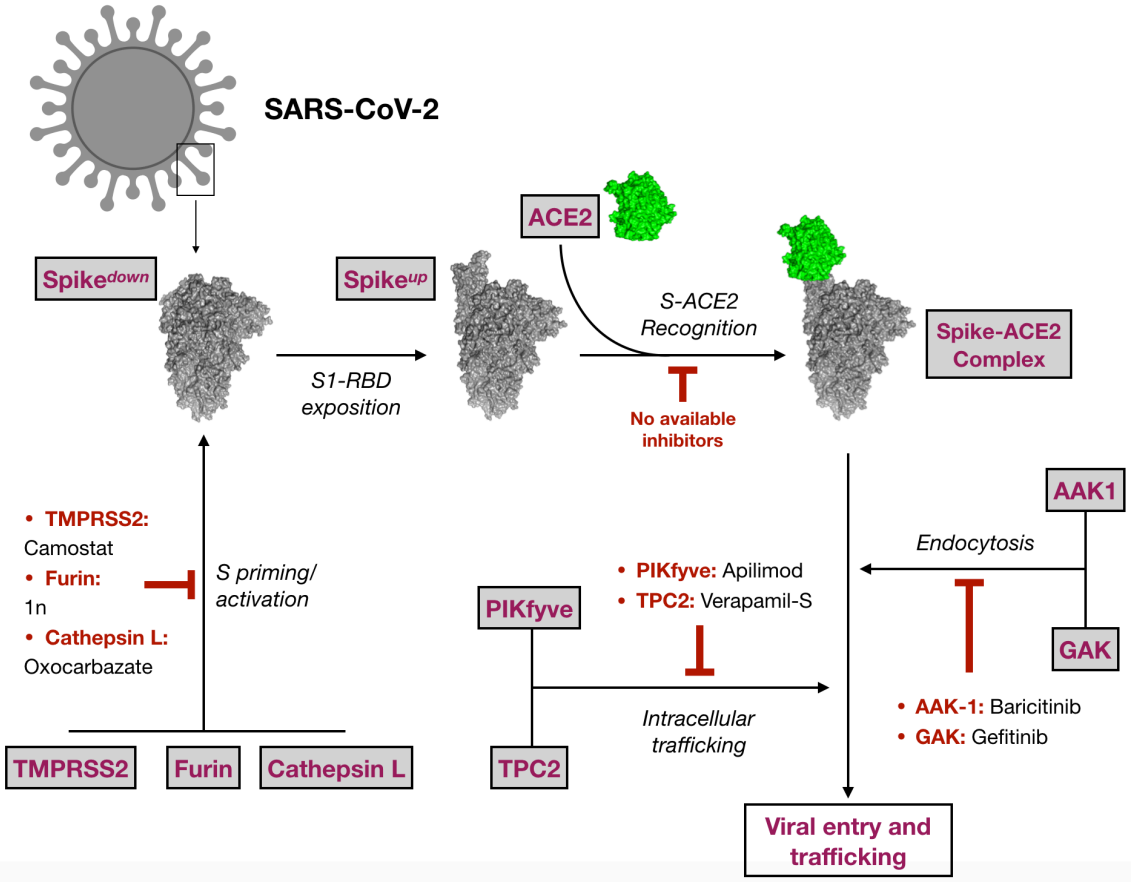

Figure 1. Schematic representation of the eight targets selected in this study and their role in virus entry. Representative inhibitors are also cited, when available.

Spike glycoprotein represents a crucial factor for virus entry and thus for virus tropism, virulence and pathogenesis (14, 15). From a structural point of view, the protein is characterized by an homotrimeric ensemble of about 1000-1200 amino acid residues per monomeric unit and is located on the outer envelope of the virion. For both SARS-CoV and SARS-CoV-2, cell-virus membrane fusion is promoted by the recognition of specific host proteins, or cell-binding agents such as the angiotensin-converting enzyme 2 (ACE2), which binds the receptor biding domain (RBD) located at the S1 subunit of the head region of the protein (15). S priming is essential to promote membranes fusion. This process is catalyzed by specific host soluble proteases, which can move and come close to S at the cell-virus interface.

The S protein of SARS-CoV-2 is cleaved at S1/S2 site by the host transmembrane serine protease 2 (TMPRSS2), a type II transmembrane serine protease of the TTSPs family, mainly expressed in the surface of the airway epithelial cells (16). TMPRSS2 was demonstrated to also cleave ACE2 (17, 18), enhancing viral infectivity. Accordingly, TMPRSS2 was proposed to enhance virus infection by simultaneously acting on (i)

ACE2 cleavage, which could promote viral uptake and (ii) S priming, which activate cell-viral membrane fusion (17, 18).

Furin pertains to the class of the calcium-dependent proprotein/prohormone convertase (PCs) and is a serine protease which is implicated in several pathological processes related to cancer, atherosclerosis and infectious diseases as those caused by Influenza A and SARS-CoV (19). Proteolytic cleavage of S is also promoted by other host proteases such as furin, which have cumulative effects of TMPRSS2-mediated S priming and SARS-CoV-2 entry (20).

Cathepsin L is a lysosomal cysteine protease of the papain family of CA (clan CA, family C1, subfamily C1A) and was recognized as responsible for the nonspecific cleavage within lysosomes. Its proteolytic activity was also linked to the propagation of several infectious diseases through the cleavage and activation of viral glycoproteins responsible for virus entry in the host cell in Ebola (21) and Hendra (22) viruses. Cathepsin L is also involved in SARS-CoV and SARS-CoV-2 S priming. *In vitro* studies demonstrated that Cathepsin L can also perform of the proteolytic activity on the Spike glycoprotein when the other host proteases mainly involved in S priming are absent (23).

All these findings highlight the pivotal role exerted by host proteases in viral infection (24, 25) thus confirming their inhibition as a valuable strategy to tackle COVID-19.

The adaptor-associated kinase 1 (AAK-1) and the cyclin G-associated kinase (GAK) represent other two interesting drug targets against SARS-CoV-2. They are members of the numb-associated kinase family (NAK) and their inhibition exerts an antiviral effect in *in vitro* assays (26, 27). NAK inhibitors exert their antiviral effect by blocking clathrin assembly necessary for clathrin-mediated endocytosis of the ACE2-bound SARS-CoV-2 particles, which are then transported to the endosome during virus entry (28).

The main endosomal phosphatidylinositol-3-phosphate/phosphatidylinositol 5-kinase (PIKfyve) was proposed to be related with intracellular trafficking of Ebola and SARS-CoV-2 viral particles (29). Moreover, the potential relevance of this target was highlighted by the antiviral effect exerted by the small PIKfyve inhibitor apilimod.

The type 2 endo-lysosomal two-pore channel (TPC2) is mainly expressed in late endosomes/lysosomes. It mediates intracellular trafficking of coronavirus through the endo-lysosomal system. Accordingly, activation of TPC2 induces a calcium-dependent depolarization of the endo-lysosomal membrane, which is supposed to enhance S-driven membrane fusion (30). In this context, TPC2 inhibitors such as verapamil (31), would be able to negatively affect depolarization thus reducing the fusogenic propensity during virus-host membrane fusion.

A list of 1789 FDA-approved drugs was screened on all the previously cited targets (see Materials and Methods section for the computational details) to find effective antiviral

compound candidates acting on SARS-CoV-2. Details about all the available PDB structures, druggable sites explored during VS and known inhibitors are reported in **Table S1** of the supporting information. The computational protocol applied in this study is shown in **Figure 2**.

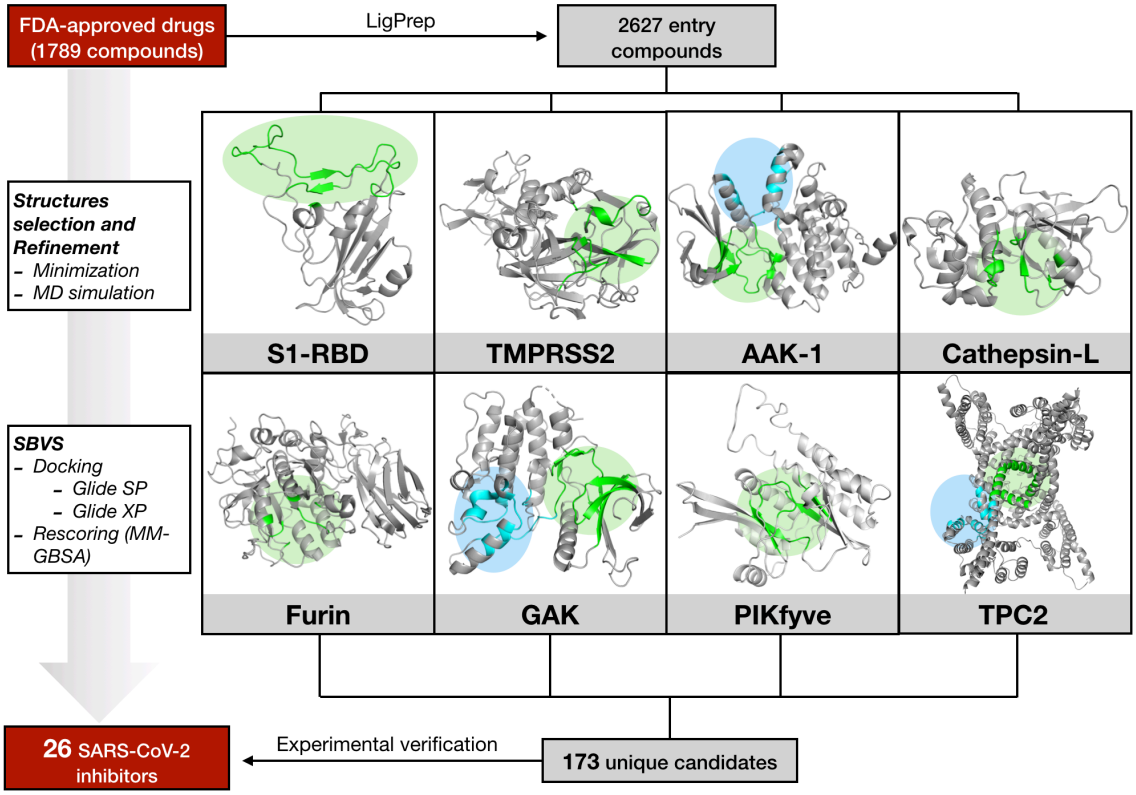

Figure 2. Schematic representation of the computational protocol applied in this study. For each target, green and blue circles respectively mark the active and the allosteric/secondary binding sites.

According to the scheme reported in **Figure 2**, all the systems were subjected to structural refinement by mean of energy minimization and the minimized structures were then used for VS. A special refinement was reserved to the S1-RBD domain of Spike and to the homology modelled structured of PIKfyve and TMPRSS2.

For PIKfyve enzyme, minimization of the homology modelled protein was realized in the presence of ATP substrate. This allowed to correctly reorient side chains for residues pertaining to the ATP binding site during minimization, preserving the geometry and shape of the cavity.

In case of S1-RBD and TMPRSS2, a further treatment based on molecular dynamic (MD) simulation in the NVT ensemble was applied. This allowed to properly explore local conformational flexibility of the ACE2 binding domain of S1-RBD and to refine the homology modelled structure of TMPRSS2 prior to virtual screening.

Trajectory analysis for S1-RBD and TMPRSS2 revealed a good stability along the MD simulation (**Figure S1** of the supporting information). For S1-RBD, a close analysis of the residues present in to the ACE2 recognition motif on the receptor binding region, revealed a mayor degree of fluctuation at the loop containing F154, N155 and Y157 (in dark blue in **Figure S1A**). Less mobility, generally lower than 1 Å, was observed in the other regions. For TMPRSS2 (**Figure S1B**), significant fluctuations were observed around the catalytic residues, H296, D345 and S441 (especially for loops in light blue, orange and green), which would be ascribable to the significant solvent exposition of the active site. For these two targets, the minimized structure and the most representative clusters (**Table S1** and **Table S2** of the supporting information) obtained from MD simulations were thus used for multi-conformation VS.

Accordingly, a total of 6 conformations for S-RBD of the Spike glycoprotein and 4 conformations for TMPRSS2 were considered for the following virtual screening (see Material and Methods section for additional information about clusters selection). For all the other targets, only the energy minimized crystallographic structure was considered (**Table S1** and **Table S2** of the supporting information).

All targets were subjected to a three-staged virtual screening protocol consisting on a preliminary docking by using the SP Glide docking algorithm, a second docking by applying the XP Glide docking algorithms and a final rescoring by applying the Prime MM-GBSA method. For each screened target, the 50 best ranked FDA drugs according to the MM-GBSA score were preliminary selected. Among them, compounds intended for a veterinary and/or cosmetic use, biocides, laxative or topical-administered drugs were not considered for SARS-CoV-2 *in vitro* assays. The complete list for the 173 selected drugs and their potential target(s) emerged from VS is shown in **Table S3** of the supporting information. These compounds were experimentally assayed for their SARS-CoV-2 antiviral potential within the framework of a *host-directed* COVID-19 antiviral therapy.

SARS-CoV-2 antiviral candidate biological evaluation: experimental screening and prioritization

Selected candidates were evaluated for their antiviral activity in a cell culture model of SARS-CoV-2 infection. Cytopathic effect was determined in Vero-E6 cells, which are particularly susceptible to SARS-CoV-2 infection with a high viral load resulting in general cell death after 72 hours of infection. This cell death can be readily delayed and even prevented by treatment with reference antiviral compounds and may be used to identify new antivirals (12). Thus, antiviral activity of new drugs can be revealed by the ability of a given compound to protect the cell monolayer upon infection. In order to

effectively determine the antiviral potential of FDA-approved drugs identified by the multi-target virtual screening described above, we tested the 173 candidates for their ability to protect Vero-E6 cells from virus-induced cell death at a fixed concentration of 10 μM. Infected cell monolayer integrity was assessed by crystal violet staining 72 hours after inoculation at a multiplicity of infection (MOI) of 0.001. This analysis revealed 26 compounds that prevented virus-induced cell death at 10 μM and 7 compounds that were cytotoxic at this concentration (**Table S3** of the supporting information).

Both sets of compounds were counterscreened in a dose-response experiment to determine the range of concentrations capable of protecting the cell monolayer and to confirm their antiviral potential (**Table S3**). Only one of the cytotoxic compounds, lanatoside C, revealed antiviral activity at lower concentrations, while the other 6 cytotoxic drugs did not reveal any protective activity. Furthermore, 5 of the primary hits (thiostrepton, dipyridamole, hycanthone, gefitinib and pirenpirone) could not be confirmed at any of the assayed doses. Thus, this study confirmed the prevention of cytopathic effect caused by SARS-CoV-2 in Vero-E6 cells of a total of 22 FDA-approved drugs and enabled the estimation of the maximum and minimum protective concentrations (PCmax and PCmin respectively), providing a preliminary assessment of the protective dose range of the 22 candidates (**Table 1**).

Table 1. Protective doses and cell viability indexes of the confirmed primary hits. PCmax and PCmin represent the maximum and minimum compound concentration (μM) able to prevent the 100% of virus-induced cytopathic effect. Highest non-toxic concentration values (μM) are inferred from the data shown in Figure S2 and represent the highest dose of compound that results in MTT values found in the vehicle-treated cells (± 20%). CC_{50} values (μM) are inferred from the same dataset.

Name	PCmax (μM)	PCmin (μM)	Highest non-toxic dose (μM)	MTT CC_{50} (μM)
Niclosamide	12.50	1.56	3.12	>50*
Loratadine	25.00	25.00	6.25	45
Ivermectin	12.50	12.50	6.25	16
Penfluridol	6.25	3.12	6.25	16
Terfenadine	12.50	12.50	12.50	18
Lapatinib	12.50	12.50	12.50	>50
Digoxin	50.00	3.70	50.00	>50
Metergoline	12.50	6.25	<0.78	12.5
Imatinib	25.00	12.50	25.00	>50*
Efloxate	50.00	25.00	50.00	>50
Ebastine	12.50	6.25	6.25	37
Posaconazole	50.00	1.25	0.78	>50*
Carvedilol	25.00	25.00	0.78	22
Protoporphyrin IX	50.00	3.70	12.50	>50*
Mycophenolate mofetil	50.00	3.12	<0.78	>50*
Pimozide	12.50	6.25	6.25	34
Tilorone hydrochloride	12.50	12.50	1.60	25
Lanatoside C	1.56	0.78	1.56	25
Cepharanthine	12.50	1.56	12.50	42
Clofazimine	50.00	6.25	50.00	>50
Reserpine	25.00	25.00	12.50	>50
Amoxapine	25.00	25.00	25.00	42

* MTT is abnormally high (>120%) after the highest normal dose and does not reach CC_{50}.

In parallel, compound cytotoxicity of the anti-SARS-CoV-2 hits was evaluated using an MTT assay to verify that protection of the cell monolayer is not associated with cytotoxicity of the compound. This assay is used to measure cellular metabolic activity as an indicator of overall cell viability, proliferation and cytotoxicity. **Table 1** summarizes also the MTT assay data shown in **Figure S2**, including the maximum drug concentration

compatible with an MTT activity comparable to that observed in the vehicle-treated cells (± 20%; highest non-toxic concentration) and the concentration at which 50% of the MTT values are reached (CC_{50}). This analysis suggested that metergoline, carvedilol and tilorone interfered significantly with cell viability and were not selected for further characterization. Several of the rest of the compounds like niclosamide, posaconazole, loratadine, mycophenolate mofetil and ivermectin showed borderline MTT values or values outside the range defined by the vehicle control (**Figure S2**), probably as a sign of metabolic adaptation to compound-induced stress. Given that the protection assay is an indirect assay that may be altered by stress-induced metabolic alterations and cytotoxicity, all the compounds with the exception of the three ones that interfered with the cell viability were subjected to direct evaluation of their antiviral activity at non-cytotoxic concentrations with antiviral potential, i.e. protective capacity.

Antiviral activity of selected candidates

In order to directly confirm the antiviral activity of the remaining 19 compounds, viral antigen expression in vehicle or candidate-treated cells was assessed by immunofluorescence microscopy using an antibody raised against SARS-CoV-2 nucleoprotein (N). Infections were carried out at a MOI of 0.01 and cells were fixed at 24 hours post inoculation, time at which no virus-induced cytopathic effect is observed. At this time of infection and MOI, the infection has locally spread in Vero-E6 and may be visualized by the expression of N protein (**Figure 3A**). Compound doses were carefully selected based on the data showed in **Figure S2** and **Table 1** to determine their antiviral potential at doses resulting in MTT assay values within the control range. Automated imaging enabled the visualization and quantification of the infection efficiency as a function of N protein expression in the presence/absence of the compounds. As shown in **Figure 3**, this analysis clearly confirmed antiviral activity of cepharantine (12.5 and 6.25 µM), protoporphyrin IX (25 and 12.5 µM) and lanatoside C (3.12 and 1.56 µM) which substantially reduced N protein accumulation in infected cells at the assayed concentrations, in a similar way as the positive control remdesivir (5 and 2.5 µM), a nucleotide analog repurposed for the treatment of SARS-CoV-2 infection (32). In addition, antiviral activity could be confirmed for one of the doses of terfenadine (12.5 µM), ebastine (12.5 µM), amoxapine (25 µM), penfluridol (6.25 µM), imatinib (25 µM), efloxate (50 µM) and pimozide (6.25 µM) while 1:2 dilution of the active concentrations was inactive in all these cases. These results suggest that, while these compounds show antiviral activity, they display a very narrow therapeutic window in cell culture. Antiviral activity could not be unequivocally demonstrated for lapatinib, reserpine, niclosamide, clofazimine or digoxin, as the selected doses reduced by less than 50% N protein

accumulation. In this sense, loratadine and ivermectin showed antiviral activity at doses where the cell number, determined by DAPI staining, was clearly reduced, suggesting that they have a measurable impact on cell viability at the active concentrations, an effect that disappears in the 1:2 dilution together with the antiviral activity. These results confirm the narrow window observed in **Figure S2** for these compounds.

These results suggest that, while protection of the cell monolayer is a valid primary readout for antiviral activity, we could not demonstrate antiviral activity for all the protective compounds. In addition, niclosamide, clofazimine or mycophenolate mofetil showed intermediate activities that required further confirmation by independent assays to confirm their antiviral potential.

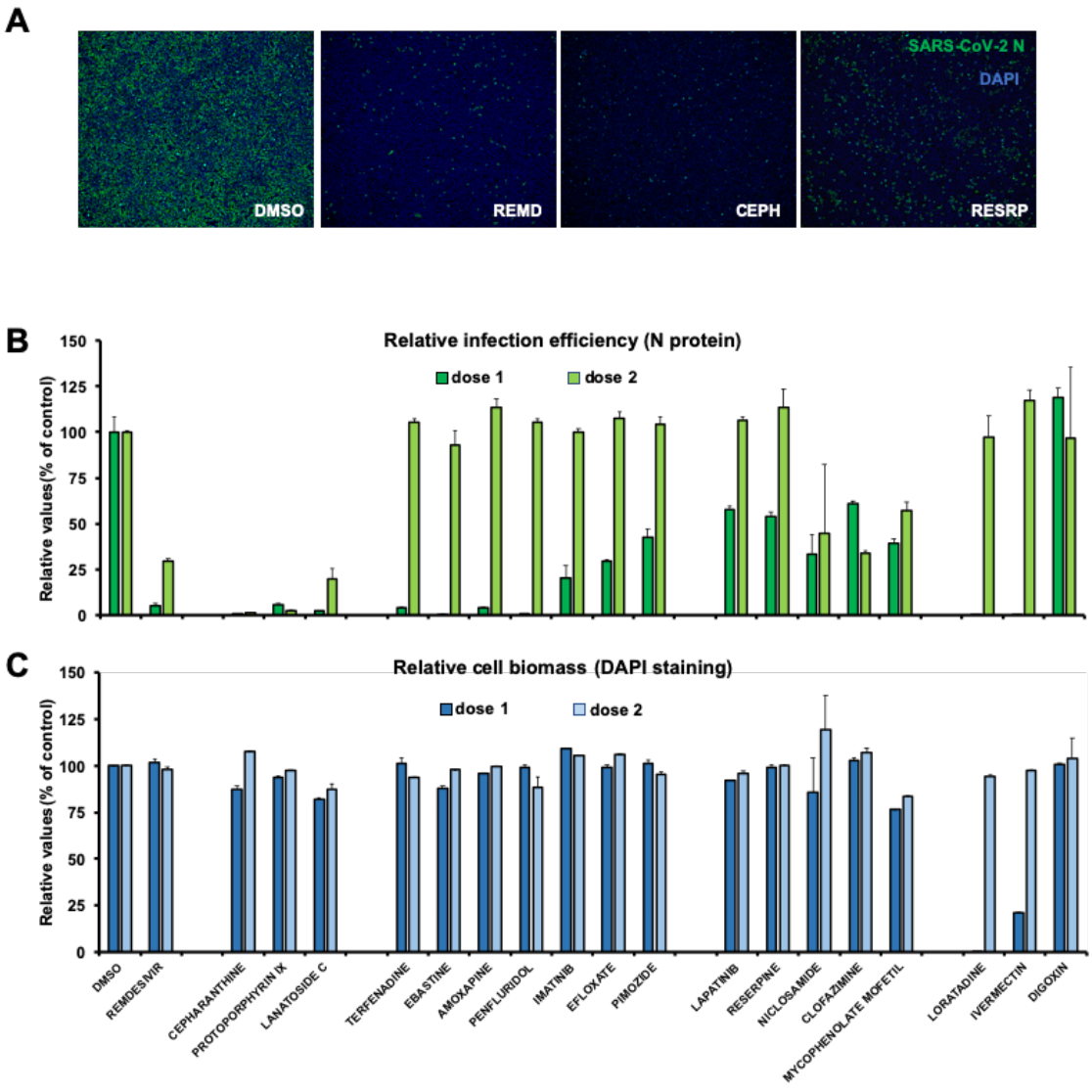

Figure 3. SARS-CoV-2 nucleoprotein (N) expression in infected Vero-E6 cells treated with the selected FDA-approved drugs. Vero-E6 cells were inoculated with SARS-CoV-2 at MOI of 0.01 in the presence of non-cytotoxic concentrations of

remdesivir (5 and 2.5 μM), cepharantine (12.5 and 6.25 μM), protoporphyrin IX (25 and 12.5 μM), lanatoside C (3.12 and 1.58 μM), terfenadine (12.5 and 6.25 μM), ebastine (12.5 and 6.25 μM), amoxapine (25 and 12.5 μM), penfluridol (6.25 and 3.12 μM), imatinib (25 and 12.5 μM), efloxate (50 and 25 μM), pimozide (6.25 and 3.12 μM), lapatinib (12.5 and 6.25 μM), reserpine (25 and 12.5 μM), niclosamide (3.12 and 1.5 μM), clofazimine (25 and 12.5 μM), mycophenolate mofetil (10 and 5 μM), loratadine (40 and 20 μM), ivermectin (12.5 and 6.25 μM) or digoxin (50 and 25 μM). After 24 hours of incubation, cells were processed for immunofluorescence microscopy analysis. A) Representative images of the immunofluoresce results with DMSO, remdesivir (REMD, 5 μM), cepharantine (CEPH, 12.5 μM) and reserpine (RESRP, 25 μM). B) Relative fluorescence values are calculated as percentage of the vehicle-treated cells. Relative infection efficiency (green bars) is estimated by the relative SARS-CoV-2 N expression. C) Relative biomass is expressed as the relative DAPI staining per well (blue bars). Data are shown as average and mean error (N=2).

Determination of viral load reduction by candidate compound treatment in SARS-CoV-2 -infected cells

To independently confirm the antiviral activity of compounds that substantially reduced infection efficiency and in order to verify the ability of the compounds to interfere with overall virus propagation, Vero-E6 cells were inoculated at MOI of 0.001 and cultured in the presence of a selection of the antiviral candidates for 48 hours, time at which total RNA was extracted to determine viral load by quantitative RT-PCR (**Figure 4**). Viral RNA accumulation in this setup is proportional to the ability of the virus to propagate in the cell monolayer in multiple rounds of infection. Viral load was reduced by more than three orders of magnitude in cells treated with the positive control, remdesivir. As expected from the reduced viral antigen expression shown in **Figure 3**, cepharantine-, lanatoside C-, and protoporphyrin IX-treated cells showed strong reduction in the viral RNA load. Similarly, antiviral doses of efloxate, imatinib and pimozide, also reduced viral RNA load, further underscoring their antiviral potential, albeit at much defined doses. On the other hand, digoxin-treated cells showed viral RNA levels comparable to those found in vehicle-treated cells, confirming that its protective activity (**Table 1**) is not associated with a measurable antiviral activity. Niclosamide-treated cells only showed a marginal reduction in viral RNA content, which together with its MTT dose-response profile precludes unambiguously concluding on the antiviral potential of this compound in cell culture. Regarding the compounds that showed intermediate activity in **Figure 3**, clofazimine treatment strongly interfered with SARS-CoV-2 propagation at several concentrations, as shown by intracellular viral RNA levels that were reduced by two

orders of magnitude at the maximum assayed concentration (50 μM; **Figure 4**). These results confirm that clofazimine shows antiviral activity at several non-cytotoxic doses and that its intrinsic fluorescence (33) may have interfered with the interpretation of the immunofluorescence results shown in **Figure 3**. In contrast, mycophenolate mofetil showed limited antiviral activity at the highest assayed concentration, underscoring the notion that this compound may interfere with viral propagation with limited efficacy in this experimental setup.

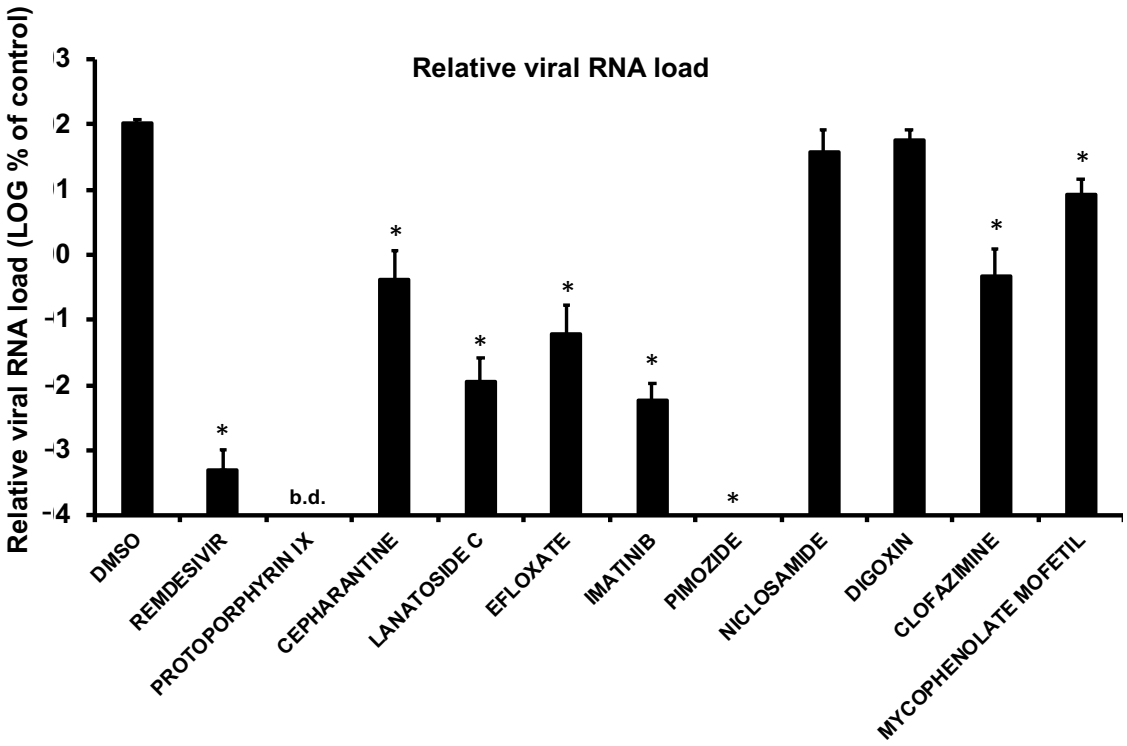

Figure 4. SARS-CoV-2 load in Vero-E6 cells after drug treatment. Vero-E6 cells were inoculated at MOI of 0.001 with SARS-CoV-2 in the presence of remdesivir (6.25 μM), protoporphyrin IX (25 μM), cepharantine (3.12 μM), lanatoside C (0.78 μM), efloxate (50 μM), imatinib (7.5 μM), pimozide (7.5 μM), niclosamide (2.5 μM), digoxin (25 μM), clofazimine (50 μM) or mycophenolate mofetil (3.12 μM). 48 hours later, total cell RNA was subjected to RT-qPCR to determine relative viral RNA load. Data are shown as average and standard deviation from three biological replicates (N=3). Statistical significance was evaluated using a one-way ANOVA and a Dunnet's post-hoc test. b. d. below detection.

Evaluation of anti-SARS-CoV-2 drugs as entry inhibitors

As the SARS-CoV-2 inhibitors described above were identified by a multi-target host-based entry targets screening, their ability to interfere with SARS-CoV-2 entry was

evaluated in a surrogate model of infection based on retroviral vectors pseudotyped with Spike envelope glycoprotein. This system encompasses the production of reporter retroviral vectors pseudotyped with the envelope glycoprotein S (Spp) which is a major determinant of SARS-CoV-2 entry, mediating receptor recognition, internalization and viral membrane fusion. This system enables evaluation of virus entry efficiency as a function of the reporter gene activity (luciferase), which is strictly dependent on the presence of a functional viral glycoprotein. As a control, pseudotypes based on vesicular stomatitis virus (VSV-G) glycoprotein were studied in parallel to determine the selectivity of the antiviral candidates. VSV-G pseudotypes use the endocytic pathway to enter the cells, although using a different receptor that S-pseudotypes and with a remarkable efficiency in many cell types (34). On the other hand, RD114-pseudotypes, also used in this study, are internalized after direct fusion of the viral envelope with the cell plasma membrane and do not follow the endocytic route (35).

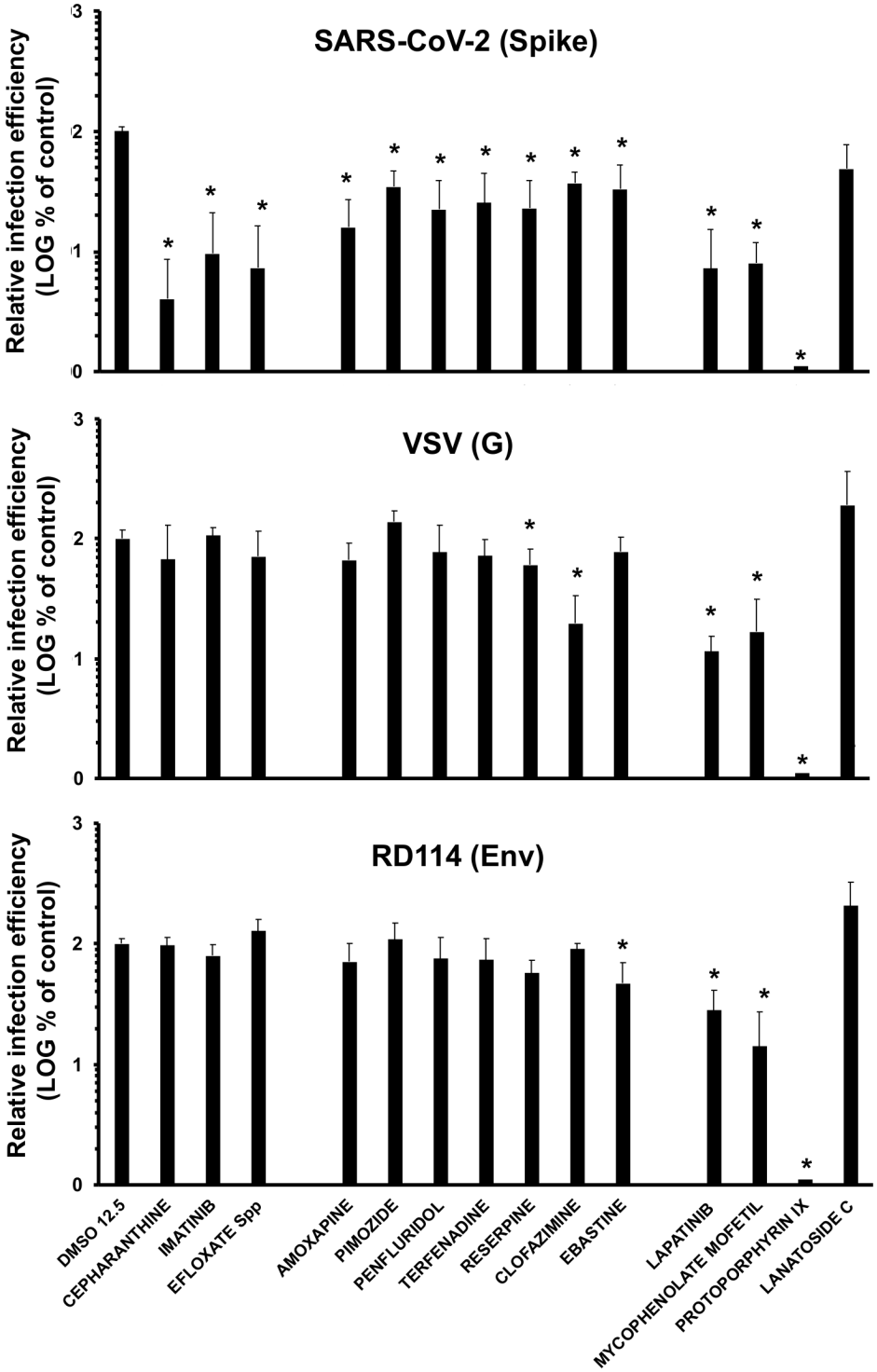

Figure 5. Antiviral candidates interfere with viral entry of SARS-CoV-2 pseudotypes. Retroviral vectors pseudotyped with envelope glycoproteins from SARS-CoV-2 (A), VSV (B) and RD114 (C) were used to inoculate Vero-E6 cells in the presence of cepharantine (6.25 µM), imatinib (12.5 µM), efloxate (50 µM), amoxapine (12.5 µM), pimozide (6.25 µM), penfluridol (6.25 µM), terfenadine (12.5 µM), reserpine (25 µM), clofazimine (50 µM), ebastine (12.5 µM), lapatinib (12.5 µM), mycophenolate mofetil (10

µM), protoporphyrin IX (12.5 µM) or lanatoside C (3.12 µM). 48 hours later, total cell lysates were assayed to determine luciferase activity as a reporter activity for viral entry. Data are shown as average and standard deviation of a minimum of two independent experiments performed in triplicate (N=6). Statistical significance was evaluated using a one-way ANOVA and a Dunnet's post-hoc test.

Analysis of the pseudotype entry efficiency shows that lapatinib, mycophenolate mofetil and protoporphyrin IX interfere with the entry assay in a non-selective manner, which precludes studying them using this system (**Figure 5**). Similarly, the results obtained with lanatoside C, were variable and inconclusive, suggesting that this compound may also interfere non-specifically with the assay (**Figure 5**).

Among the rest of the tested compounds, cepharantine, imatinib and efloxate showed the greatest antiviral activity and relative selectivity for Spp entry as compared with the controls (**Figure 5**), indicating that they are indeed SARS-CoV-2 entry inhibitors. Amoxapine, pimozide, penfluridol, terfenadine and reserpine, inhibit Spp entry by 3-5 folds as compared with the vehicle, and only marginally interfere with entry of the control pseudotypes VSVpp and RD114pp. In this sense, reserpine, terfenadine, clofazimine (VSVpp) and ebastine (RD114pp) caused a statistically significant difference with one of the control pseudotypes (**Figure 5**) but with a magnitude that can be distinguished from that observed in Spp, suggesting some degree of selectivity. This reduced selectivity probably reflects the small therapeutic window observed for these compounds (**Table 1** and **Figure 3**).

Overall, our results support the notion that the compounds selected by the screening procedure described above, with the exception of lapatinib, mycophenolate mofetil, protoporphyrin IX and lanatoside C, inhibit SARS-CoV-2 infection by interfering with viral entry in a partially selective manner.

DISCUSSION

Since its first detection in December 2019 in Wuhan, the capital of China's Hubei province, COVID-19 has spread worldwide rapidly. The outbreak was declared a Public Health Emergency by WHO on 30 January 2020 and since then, utmost efforts were made by the international scientific community in the attempt to find an effective cure. The full characterization of the SARS-CoV-2 viral genome by Fuk-Woo Chan J. and collaborators (36), followed by crystallization of most of its viral components offered the structural bases to search for an effective treatment.

Vaccines represent the gold standard long-term choice to fight SARS-CoV-2 pandemic and COVID-19. Given the lack of such vaccine, pharmacological treatment of the

infections with small molecules is a valid approach, but it is affected by important disadvantages, such as low potency and emergence of drug-resistant virus variants, especially when applied as monotherapy. These limitations could be dampened by the application of broad-spectrum antiviral agents simultaneously acting on more than one target at the same time (37). Furthermore, to reduce the likelihood of resistance in future treatments, the design of antivirals able to block host targets involved in viral infection is an emerging and promising strategy (38). In fact, this is the approach followed in this study. Thus, we screened *in silico* the same chemical library against eight different entry SARS-CoV-2 targets, being all of them human proteins.

Specifically, to fight against COVID-19 great attention was paid to molecular events associated to virus entry, which are primarily mediated by the S glycoprotein. According to recent studies, S protein of SARS-CoV-2 is translated into an uncleaved and inactive form (S0) (39), which is generally activated by proteolytic cleavage by host proteases such as TMPRSS2 during protein egress (15). Once primed and exposed on the viral membrane, the fusion event can occur and is initiated by recognition of specific host receptors as ACE2 (39) by the receptor binding domain (S1-RBD), located at the S1 subunit of the protein. The priming activity can also be managed by other host proteases as furin, and Cathepsin L in a compensatory mechanism. After host-virus recognition, the viral material is internalized by endocytosis and trafficked into the host cell. This process is mediated by several host factors, which are currently a matter of intense investigation for their pharmacological suitability as anti-SARS-CoV-2 targets.

In this direction, inhibitors of the host proteases TMPRSS2, furin and Cathepsin L, the kinases AAK-1, GAK and PIKfyve as well as TPC2 ion channel may offer the possibility to act at different levels during virus attachment, endocytosis and trafficking.

Following this trend, a hierarchical host-directed virtual screening protocol was applied to select potential anti-SARS-CoV-2 drugs based on the above-mentioned host targets with the aim to find a host-based therapy for COVID-19 capable to interfere with virus attachment, endocytosis and trafficking. In this regard, 173 FDA approved drugs were selected from the multi-target *in silico* virtual screening conducted on a library of 1789 drugs and finally tested against SARS-CoV-2 viral infection using a high-throughput screening (HTS) protocol which was optimized for this work.

The potential antiviral activity of the 173 FDA-approved drugs selected during VS was first evaluated in a cell culture model of SARS-CoV-2 infection at a fixed concentration of 10 μM. Vero-E6 cells were selected because of the proven susceptibility to the infection by this coronavirus. This preliminary assay yielded 26 hits (**Table S3**) and subsequent dose-response experiment to determine the range of protective concentration allowed the confirmation of 22 candidates for further studies (**Table 1**).

The next step in the characterization of our drug candidates was the determination of maximum and minimum compound concentration where cells are protected from SARS-CoV-2-induced cell death (PCmax and PCmin) together with the cytotoxic concentration (CC_{50}) by MTT assay in order to determine the therapeutic window of the candidates (**Table 1**). From these assays, the five drugs imatinib, protoporphyrin IX, lanatoside C, cepharantine and clofazimine showed a clear protective activity at non-toxic concentrations, while other three, posaconazole, carvedilol and tilorone, were discarded for further characterization due to the clear lack of therapeutic window in the experimental conditions used. These drugs were proposed in the literature as potential anti-COVID19 agents based mainly on their primary mechanism of action, but none of them was tested previously against SARS-CoV-2 (40, 41). In the case of tilorone, no therapeutic window was found, thus precluding demonstrating antiviral activity in this cell culture system, which is in line with other already published reports (11).

Confirmation of antiviral activity for the 19 selected compounds was performed by immunofluorescence microscopy using an antibody capable of detecting SARS-CoV-2 nucleoprotein (N) in infected cells and intracellular viral RNA quantification by RT-qPCR. Results from both experiments (**Figures 3** and **4**) confirmed that except for loratadine, ivermectin, niclosamide and digoxin, the rest of the compounds showed viral inhibition at non-toxic concentrations. Surprisingly, the lack of antiviral activity found for ivermectin, which was hypothesized to inhibit ACE2-S-RBD interaction according to our VS, contrasts with the antiviral activity on SARS-CoV-2 clinical isolate Australia/VIC01/2020 reported in Vero/hSLAM cells (42). Further clinical trials of ivermectin for COVID-19 are ongoing (43), and only these results when available will assess the anti-SARS-CoV-2 efficacy of this broad spectrum antiparasitic agent. Curiously, no clinical benefit was reported in a recent phase III study of ivermectin in Thailand conducted on dengue virus-infected patients (44).

Finally, a specific assay consisting on S protein pseudotyped retroviral vectors was set up to gain deeper knowledge about the potential ability of identified antivirals to inhibit SARS-CoV-2 entry. In these experiments, VSV-G and RD114 pseudotypes were used as controls. VSV-G pseudotypes use the endocytic pathway to enter the cells through a different receptor that S-pseudotypes. RD114-pseudotypes are internalized after direct fusion of the viral envelope with the cell plasma membrane. Overall, the results of the pseudotype entry efficiency (**Figure 5**) indicated that all the selected drugs inhibit SARS-CoV-2 infection by interfering with viral entry. Among those, cepharantine, imatinib and efloxate were the best compounds and displayed a superior selectivity as compared with the rest of the entry inhibitors.

Cepharantine was approved in Japan to treat alopecia (45), which was proposed in the last months as anti-COVID-19 therapy based on theoretical and *in vitro* results (11). Our *in silico* results showed that cepharantine could be a potential inhibitor of furin and TPC2, being its biological action involved not only in first entry phases but also in the escape from late endosomes, a mechanism that is compatible with the results obtained in the surrogate model of viral entry here presented.

Due to the involvement of Abl pathway in viral infections, imatinib was proposed as anti-SARS-CoV-2 and clinical trials were started since the first moment of the pandemic (46), although no experimental evidence of antiviral activity was reported. At the time of writing this manuscript *in vitro* activity against SARS-CoV-2 has been described (47) in agreement with the results here presented.

As far as we know, no antiviral activity has ever been reported for the vasodilator efloxate. Our virtual screening shows that this drug could potentially inhibit AAK1 and GAK kinases involved in early endosome entry.

Moreover, we have already shown that protoporphyrin IX and lanatoside C have also good antiviral properties although their mechanism of action is not mediated by the inhibition of the viral entry pathway. Both compounds have been previously described as anti-SARS-CoV-2 agents in different studies (11, 48). Clofazimine, used as an antimicrobial agent, also showed consistent antiviral activity and interfered significantly with Spp and VSVpp but not RD114pp infection, suggesting a non-selective impact on viral entry through the endosomal route.

Overall, the use of an FDA-approved chemical library allowed us to check the robustness and reproducibility of our protocol, a multi-target virtual screening following by a solid experimental cascade of biological assays. Our study allowed the identification and experimental validation of valuable candidates to be repurposed as potential COVID-19 therapy such as cepharantine, efloxate, imatinib, protoporphyrin IX, clofazimine and lanatoside C. Moreover, a potential mechanism of action for these drugs was also proposed by *in silico* VS analyses as they would be able to modulate some of the host proteins involved in the entry process of SARS-CoV-2 and was experimentally validated for cepharantine, efloxate and imatinib.

In summary, we have identified a list of six drugs ready to be validated in clinical trials as SARS-CoV-2 infection inhibitors. In case of positive results from clinical trials with COVID-19 patients, these compounds may promote a new era of antiviral agents potentially able to combat the current COVID-19 pandemic, but also future outbreaks of high pathogenic viruses, which would share a common entry pathway as infection mechanism.

MATERIALS AND METHODS

Computational studies

The drug-dataset. A starting list of 1789 FDA-approved drugs (US Drug Collection, MicroSource Discovery Systems) has been prepared for VS with the LigPrep and Epik modules of Maestro suite (49). Accordingly, all possible ionization states at pH 7.2 ± 2.0 have been predicted for each compound. Original chirality has been retained. This led to a total of 2627 compounds. The force field, OPLS3 (50) has been used to define all the generated compounds.

Protein targets and MD simulations. The X-ray crystal structure of SARS-CoV-2 spike receptor binding domain in complex with ACE2 (PDB ID: 6M0J) (51) has been used as model for the S1-RBD-ACE2 recognition surface.

For TMPRSS2, the homology modelled extracellular region of the protein was obtained from the Swiss-Model repository (52). The model was obtained from the serine protease hepsin (PDB ID: 5CE1), which shares the 34% of sequence identity with the target protein, TMPRSS2.

Amber 18 (53) was used to explore the local conformational flexibility of the S1-RBD of Spike and to refine the homology modelled structure of TMPRSS2. The ff14SB force field (54) was used to define the proteins which were embedded in a truncated octahedral TIP3P (55) water box in a layer of 22 Å and neutralized by adding chlorine counterions. Disulphide bonds were built by using the “bond” command in tleap.

Protonation states for titratable residues were set according to Propka (56) predictions at pH 7.3. Systems were energy minimized in three steps involving firstly all hydrogen atoms, then water molecules, and finally all the system. For the final step, a maximum of 50,000 (5,000 iterations with steepest descent and the rest with conjugate gradient) were run. Thermalization of the minimized systems from 0 to 300 K was accomplished in five steps, the first being performed at constant volume and the rest at constant pressure. Langevin dynamics with a collision frequency of 1.0 ps^{-1} was applied for temperature regulation during thermalization. Prior to MD, 5 ns of equilibration at constant pressure were run to properly stabilize the systems. A total of 100 ns of MD production were generated in the NVT ensemble and in periodic boundary conditions for both systems. A time step of 2 fs was set for saving trajectories.

The SHAKE algorithm (57) was applied to constrain bonds involving hydrogen atoms. Cut-off for non-bonded interactions was set to 10 Å. Electrostatic interactions beyond the cut-off within the periodic box were computed by applying the Particle Mesh Ewald (PME) method (58). The weak-coupling algorithm with a time constant of 10.0 ps was used to stabilize the temperature during the simulation. Trajectories analysis and clusterization were done by using the CPPTRAJ module of Amber18. For clustering analysis, a total

of 10 clusters were preliminary searched by using the average linkage algorithm, which uses the average distance between members of two clusters (59). Representative structure for each cluster was represented by the average structure. Cut-off for determining local density was set at 4 angstroms. Parameters for clusterization were adapted considering both trajectory and protein length.

For human PIKfyve, the structure of the protein has been obtained by homology modeling by using the crystal structure of zebrafish Phosphatidylinositol-4-phosphate 5-kinase alpha isoform with bound ATP/Ca^{2+} (PDEB code: 6CMW), which shares the 28% of global sequence identity (60). To proper refine the ATP binding site in the homology modelled PIKfyve enzyme, ATP has been accommodated in its binding site by using the template complex as reference and the so derived PIKfyve-ATP complex has been then energy minimized. The ATP parameters for minimization with Amber18 were taken from the Amber parameter database of the Bryce group (61, 62). The complete list for all the crystallographic structures used during VS is reported in **Table S1**.

Structure-based Virtual Screening (SBVS) and MM-GBSA rescoring. The complete FDA database of 1789 approved drugs was screened against the previously described targets. Representative 3D-structures/clusters for S1-RBD and TMPRSS2 were selected from MD simulations. For cluster selection on S-RBD, clusters with a population higher than 5% (clusters 0-4) were considered for VS with the aim to enhance the exploration of the conformational variability of the receptor binding site of S protein. In case of TMPRSS2, only those clusters were the active site was in an open state were considered, 3 clusters (cluster 0-2) were finally selected for VS. For both systems, the minimized structure was also considered for VS.

For the rest of the screened systems (AAK-1, Cathepsin-L, furin, GAK, PIKfyve and TPC2), the minimized crystallographic structures were prepared for virtual screening with the protein preparation wizard from the Maestro suite, applying the OPLS3e force field (50) with default parameters. The grid boxes were centered on the active site for each target (see **Table S1**) using default parameters for receptor grid generation.

SBVS was then performed by using a pipeline which included 3 stages. The first one consisted in massive docking simulations employing the Glide software (63) and the Standard Precision (SP) method. In this first stage, an enhanced sampling approach was used, and 5 poses were generated per compound state. The best 50% of compounds (according to the scoring function) were kept and used for the second stage, where the Extra Precision (XP) method was employed. In the second stage, 25% of the best-ranked solutions were kept. Rescoring was performed in the third stage with Prime MM-GBSA method (64).

SARS-CoV-2 infection assays

All infection experiments were performed by inoculating Vero-E6 cells seeded onto 96-well plates ($2x10^4$ cells/well) with the SARS-CoV-2 strain NL/2020 (kindly provided by Dr. R. Molenkamp, Erasmus University Medical Center Rotterdam) at low multiplicity of infection (MOI) of 0.01 or 0.001, as indicated below. Cultures were maintained at 37 ºC in a 5% CO_2 incubator for different lengths of time depending on the experiment. Compounds were diluted from 10 mM stock solutions in complete media containing 2% FBS to achieve the indicated final concentrations.

Cell monolayer protection assays: Vero-E6 cell monolayers were inoculated at MOI 0.001 in the presence of 10 µM of each compound in duplicate wells. Seventy-two hours later the cells were fixed and stained using crystal violet. Compounds that protect from the virus induced cell death were selected for further experiments. A wide range of compound concentrations (from 50 to 0.78 µM) from the selected compounds were used in subsequent experiments to determine the maximum and minimum protective concentration (PCmax and PCmin) as indicated above.

Cytotoxicity measurement by MTT assays: Vero-E6 cell monolayers were treated with a wide range of compound concentrations (from 50 to 0.78 µM) and forty-eight hours later they were subjected to MTT assays following the manufacturer's instructions.

Intracellular viral RNA quantitation: To confirm that protection of the monolayer was indeed due to the ability of the compounds to restrict virus replication, viral RNA quantitation was performed as indicated below. Vero-E6 cell monolayers were inoculated at MOI 0.001 in the presence of the indicated compound concentrations. Forty-eight hours later cell lysates were prepared using Trizol reagent (Thermo Scientific). Viral RNA content was determined by RT-qPCR using previously validated sets of primers and probes specific for the detection of the SARS-CoV-2 E gene (65) and the cellular 28S RNA for normalization purposes. ΔCt method was used for relative quantitation of the intracellular viral RNA accumulation in compound-treated cells compared to the levels in infected cells treated with DMSO, set as 100%.

Hit validation by immunofluorescence microscopy.

VeroE6 were seeded onto 96-well plates as described above and infected in the presence of the indicated compound dose (MOI 0.01). Twenty-four hours post infection, cells were fixed for 20 minutes at RT with a 4% formaldehyde solution in PBS, washed twice with PBS and incubated with incubation buffer (3% BSA; 0.3% Triton X100 in PBS) for 1 hour. A monoclonal antibody against N protein was diluted in incubation buffer (1:2000; Genetex HL344) and incubated with the cells for 1 hour, time after which the cells were washed with PBS and subsequently incubated with a 1:500 dilution of a goat anti-mouse conjugated to Alexa 488 (Invitrogen-Carlsbad, CA). Nuclei were stained with

DAPI (Life Technologies) during the secondary antibody incubation using the manufacturer´s recommendations. Cells were washed with PBS and imaged using an automated multimode reader (TECAN Spark Cyto; Austria).

SARS-CoV-2 Spike protein-pseudotyped retroviral vectors

Retroviral particle production pseudotyped with different viral envelopes has previously been described (66, 67). Packaging plasmids, vesicular stomatitis virus (VSV) G and RD114 glycoprotein expressing plasmids were kindly provided by Dr. F. L. Cosset (INSERM, Lyon). SARS-CoV-2 S expressing plasmid was obtained from Jose María Casanovas and Juan García Arriaza (CNB-CSIC). Particles devoid of envelope glycoproteins were produced in parallel as controls.

For SARS-CoV-2 Spike pseudotyped particle (SARS2pp) entry experiments, Vero-E6 cells (10^4 cells/well) were seeded onto 96-well plates the day before. Compounds were diluted in complete media [(DMEM supplemented with 10 mM HEPES, 1x non-essential amino acids (Gibco), 100 U/ mL penicillin-streptomycin (Gibco) and 10% Fetal Bovine Serum (heat-inactivated at 56 ºC for 30 min)] to achieve a 2x concentration. Fifty microliters (50 µL) of the SARS2pp, VSVpp or RD114 retrovirus dilutions were mixed 1:1 with 50 µL of the 2x compound dilutions to achieve the desired final compound concentrations, as indicated in the figure. One hundred µL of the mixture was applied onto the Vero E6 cell monolayer in biological triplicates and cells were cultured at 37 ºC in a 5% CO_2 incubator. Forty-eight hours post-inoculation, cells were lysed for luciferase activity determination using Luciferase Assay System (Promega) and a luminometer. Relative infection values were determined by normalizing the data to the average relative light units detected in the vehicle control cells.

Acknowledgments

Funding from CSIC (201980E024, 202020E103 and PIE-RD-COVID-19 ref. E202020E079), EVA (European Virus Archive; grant agreement Nº 871029), FONDECYT grant Nº 11180604 and CONICYT-PCI grant Nº REDES190074 is acknowledged. Dr. R. Molenkamp (Erasmus University Medical Center, Rotterdam, Netherlands; participant of the EVA-GLOBAL project) is acknowledged for the SARS-CoV-2 strain NL/2020 virus. Dr. F. L. (Inserm-Lyon) is acknowledged for the materials required to produce retroviral pseudotypes.

References

1. Zhou P, Yang XL, Wang XG, Hu B, Zhang L, Zhang W, Si HR, Zhu Y, Li B, Huang CL, Chen HD, Chen J, Luo Y, Guo H, Jiang RD, Liu MQ, Chen Y, Shen XR, Wang X, Zheng XS, Zhao K, Chen QJ, Deng F, Liu LL, Yan B, Zhan FX, Wang YY, Xiao GF, Shi ZL. 2020. A pneumonia outbreak associated with a new coronavirus of probable bat origin. Nature 579:270-273.
2. Saul S, Einav S. 2020. Old drugs for a new virus: Repurposed approaches for combating COVID-19. ACS Infect Dis 6:2304-2318.
3. Pan H, Peto R, Karim QA, Alejandria M, Henao-Restrepo AM, García CH, Kieny M-P, Malekzadeh R, Murthy S, Preziosi M-P, Reddy S, Periago MR, Sathiyamoorthy V, Røttingen J-A, Swaminathan S. 2020. Repurposed antiviral drugs for COVID-19 –interim WHO SOLIDARITY trial results. medRxiv doi:10.1101/2020.10.15.20209817.
4. https://www.fda.gov/news-events/press-announcements/coronavirus-covid-19-update-fda-issues-emergency-use-authorization-potential-covid-19-treatment (accessed November 17, 2020).
5. Mulangu S, Dodd LE, Davey RT, Jr., Tshiani Mbaya O, Proschan M, Mukadi D, Lusakibanza Manzo M, Nzolo D, Tshomba Oloma A, Ibanda A, Ali R, Coulibaly S, Levine AC, Grais R, Diaz J, Lane HC, Muyembe-Tamfum JJ, Group PW, Sivahera B, Camara M, Kojan R, Walker R, Dighero-Kemp B, Cao H, Mukumbayi P, Mbala-Kingebeni P, Ahuka S, Albert S, Bonnett T, Crozier I, Duvenhage M, Proffitt C, Teitelbaum M, Moench T, Aboulhab J, Barrett K, Cahill K, Cone K, Eckes R, Hensley L, Herpin B, Higgs E, Ledgerwood J, Pierson J, Smolskis M, Sow Y, Tierney J, Sivapalasingam S, Holman W, Gettinger N, et al. 2019. A randomized, controlled trial of Ebola virus disease therapeutics. N Engl J Med 381:2293-2303.
6. Ashburn TT, Thor KB. 2004. Drug repositioning: identifying and developing new uses for existing drugs. Nat Rev Drug Discov 3:673-683.
7. Zheng W, Sun W, Simeonov A. 2018. Drug repurposing screens and synergistic drug-combinations for infectious diseases. Br J Pharmacol 175:181-191.
8. Pushpakom S, Iorio F, Eyers PA, Escott KJ, Hopper S, Wells A, Doig A, Guilliams T, Latimer J, McNamee C, Norris A, Sanseau P, Cavalla D, Pirmohamed M. 2019. Drug repurposing: progress, challenges and recommendations. Nat Rev Drug Discov 18:41-58.
9. Mercorelli B, Palu G, Loregian A. 2018. Drug repurposing for viral infectious diseases: How far are we? Trends Microbiol 26:865-876.

10. Gil C, Ginex T, Maestro I, Nozal V, Barrado-Gil L, Cuesta-Geijo MA, Urquiza J, Ramirez D, Alonso C, Campillo NE, Martinez A. 2020. COVID-19: Drug targets and potential treatments. J Med Chem 63:12359–12386.
11. Jeon S, Ko M, Lee J, Choi I, Byun SY, Park S, Shum D, Kim S. 2020. Identification of antiviral drug candidates against SARS-CoV-2 from FDA-approved drugs. Antimicrob Agents Chemother 64:e00819-20.
12. Riva L, Yuan S, Yin X, Martin-Sancho L, Matsunaga N, Pache L, Burgstaller-Muehlbacher S, De Jesus PD, Teriete P, Hull MV, Chang MW, Chan JF, Cao J, Poon VK, Herbert KM, Cheng K, Nguyen TH, Rubanov A, Pu Y, Nguyen C, Choi A, Rathnasinghe R, Schotsaert M, Miorin L, Dejosez M, Zwaka TP, Sit KY, Martinez-Sobrido L, Liu WC, White KM, Chapman ME, Lendy EK, Glynne RJ, Albrecht R, Ruppin E, Mesecar AD, Johnson JR, Benner C, Sun R, Schultz PG, Su AI, Garcia-Sastre A, Chatterjee AK, Yuen KY, Chanda SK. 2020. Discovery of SARS-CoV-2 antiviral drugs through large-scale compound repurposing. Nature 586:113-119.
13. Guy RK, DiPaola RS, Romanelli F, Dutch RE. 2020. Rapid repurposing of drugs for COVID-19. Science 368:829-830.
14. Ou X, Liu Y, Lei X, Li P, Mi D, Ren L, Guo L, Guo R, Chen T, Hu J, Xiang Z, Mu Z, Chen X, Chen J, Hu K, Jin Q, Wang J, Qian Z. 2020. Characterization of spike glycoprotein of SARS-CoV-2 on virus entry and its immune cross-reactivity with SARS-CoV. Nat Commun 11:1620.
15. Walls AC, Park YJ, Tortorici MA, Wall A, McGuire AT, Veesler D. 2020. Structure, function, and antigenicity of the SARS-CoV-2 spike glycoprotein. Cell 181:281-292 e6.
16. Kam YW, Okumura Y, Kido H, Ng LF, Bruzzone R, Altmeyer R. 2009. Cleavage of the SARS coronavirus spike glycoprotein by airway proteases enhances virus entry into human bronchial epithelial cells in vitro. PLoS One 4:e7870.
17. Heurich A, Hofmann-Winkler H, Gierer S, Liepold T, Jahn O, Pohlmann S. 2014. TMPRSS2 and ADAM17 cleave ACE2 differentially and only proteolysis by TMPRSS2 augments entry driven by the severe acute respiratory syndrome coronavirus spike protein. J Virol 88:1293-1307.
18. Shulla A, Heald-Sargent T, Subramanya G, Zhao J, Perlman S, Gallagher T. 2011. A transmembrane serine protease is linked to the severe acute respiratory syndrome coronavirus receptor and activates virus entry. J Virol 85:873-882.
19. Dahms SO, Jiao GS, Than ME. 2017. Structural studies revealed active site distortions of human Furin by a small molecule inhibitor. ACS Chem Biol 12:1211-1216.

20. Shang J, Wan Y, Luo C, Ye G, Geng Q, Auerbach A, Li F. 2020. Cell entry mechanisms of SARS-CoV-2. Proc Natl Acad Sci U S A 117:11727-11734.
21. Brecher M, Schornberg KL, Delos SE, Fusco ML, Saphire EO, White JM. 2012. Cathepsin cleavage potentiates the Ebola virus glycoprotein to undergo a subsequent fusion-relevant conformational change. J Virol 86:364-372.
22. Pager CT, Dutch RE. 2005. Cathepsin L is involved in proteolytic processing of the Hendra virus fusion protein. J Virol 79:12714-12720.
23. Bosch BJ, Bartelink W, Rottier PJ. 2008. Cathepsin L functionally cleaves the severe acute respiratory syndrome coronavirus class I fusion protein upstream of rather than adjacent to the fusion peptide. J Virol 82:8887-8890.
24. Hardes K, Becker GL, Lu Y, Dahms SO, Kohler S, Beyer W, Sandvig K, Yamamoto H, Lindberg I, Walz L, von Messling V, Than ME, Garten W, Steinmetzer T. 2015. Novel Furin inhibitors with potent anti-infectious activity. ChemMedChem 10:1218-1231.
25. Shah PP, Wang T, Kaletsky RL, Myers MC, Purvis JE, Jing H, Huryn DM, Greenbaum DC, Smith AB, 3rd, Bates P, Diamond SL. 2010. A small-molecule oxocarbazate inhibitor of human cathepsin L blocks severe acute respiratory syndrome and ebola pseudotype virus infection into human embryonic kidney 293T cells. Mol Pharmacol 78:319-324.
26. Bekerman E, Neveu G, Shulla A, Brannan J, Pu SY, Wang S, Xiao F, Barouch-Bentov R, Bakken RR, Mateo R, Govero J, Nagamine CM, Diamond MS, De Jonghe S, Herdewijn P, Dye JM, Randall G, Einav S. 2017. Anticancer kinase inhibitors impair intracellular viral trafficking and exert broad-spectrum antiviral effects. J Clin Invest 127:1338-1352.
27. Stebbing J, Phelan A, Griffin I, Tucker C, Oechsle O, Smith D, Richardson P. 2020. COVID-19: combining antiviral and anti-inflammatory treatments. Lancet Infect Dis 20:400-402.
28. Gordon DE, Jang GM, Bouhaddou M, Xu J, Obernier K, White KM, O'Meara MJ, Rezelj VV, Guo JZ, Swaney DL, Tummino TA, Huettenhain R, Kaake RM, Richards AL, Tutuncuoglu B, Foussard H, Batra J, Haas K, Modak M, Kim M, Haas P, Polacco BJ, Braberg H, Fabius JM, Eckhardt M, Soucheray M, Bennett MJ, Cakir M, McGregor MJ, Li Q, Meyer B, Roesch F, Vallet T, Mac Kain A, Miorin L, Moreno E, Naing ZZC, Zhou Y, Peng S, Shi Y, Zhang Z, Shen W, Kirby IT, Melnyk JE, Chorba JS, Lou K, Dai SA, Barrio-Hernandez I, Memon D, Hernandez-Armenta C, et al. 2020. A SARS-CoV-2 protein interaction map reveals targets for drug repurposing. Nature 583:459-468.

29. Kang YL, Chou YY, Rothlauf PW, Liu Z, Soh TK, Cureton D, Case JB, Chen RE, Diamond MS, Whelan SPJ, Kirchhausen T. 2020. Inhibition of PIKfyve kinase prevents infection by Zaire ebolavirus and SARS-CoV-2. Proc Natl Acad Sci U S A 117:20803-20813.
30. Filippini A, D'Amore A, Palombi F, Carpaneto A. 2020. Could the inhibition of endo-lysosomal two-pore channels (TPCs) by the natural flavonoid naringenin represent an option to fight SARS-CoV-2 infection? Front Microbiol 11:970.
31. Gunaratne GS, Yang Y, Li F, Walseth TF, Marchant JS. 2018. NAADP-dependent Ca(2+) signaling regulates Middle East respiratory syndrome-coronavirus pseudovirus translocation through the endolysosomal system. Cell Calcium 75:30-41.
32. Williamson BN, Feldmann F, Schwarz B, Meade-White K, Porter DP, Schulz J, van Doremalen N, Leighton I, Yinda CK, Pérez-Pérez L, Okumura A, Lovaglio J, Hanley PW, Saturday G, Bosio CM, Anzick S, Barbian K, Cihlar T, Martens C, Scott DP, Munster VJ, de Wit E. 2020. Clinical benefit of remdesivir in rhesus macaques infected with SARS-CoV-2. Nature 585:273-276.
33. Baik J, Rosania GR. 2011. Molecular imaging of intracellular drug-membrane aggregate formation. Mol Pharm 8:1742-1749.
34. Sun X, Roth SL, Bialecki MA, Whittaker GR. 2010. Internalization and fusion mechanism of vesicular stomatitis virus and related rhabdoviruses. Future Virol 5:85-96.
35. Rasko JE, Battini JL, Gottschalk RJ, Mazo I, Miller AD. 1999. The RD114/simian type D retrovirus receptor is a neutral amino acid transporter. Proc Natl Acad Sci U S A 96:2129-2134.
36. Chan JF, Kok KH, Zhu Z, Chu H, To KK, Yuan S, Yuen KY. 2020. Genomic characterization of the 2019 novel human-pathogenic coronavirus isolated from a patient with atypical pneumonia after visiting Wuhan. Emerg Microbes Infect 9:221-236.
37. Debing Y, Neyts J, Delang L. 2015. The future of antivirals: broad-spectrum inhibitors. Curr Opin Infect Dis 28:596-602.
38. Kumar N, Sharma S, Kumar R, Tripathi BN, Barua S, Ly H, Rouse BT. 2020. Host-directed antiviral therapy. Clin Microbiol Rev 33:e00168-19.
39. Coutard B, Valle C, de Lamballerie X, Canard B, Seidah NG, Decroly E. 2020. The spike glycoprotein of the new coronavirus 2019-nCoV contains a furin-like cleavage site absent in CoV of the same clade. Antiviral Res 176:104742.
40. Ayoub N. 2020. Carvedilol as a potential addition to the COVID-19 therapeutic arsenal. Int J Pharm Pharm Sci 12:87-89.

41. Sturley SL, Rajakumar T, Hammond N, Higaki K, Márka Z, Márka S, Munkacsi AB. 2020. Potential COVID-19 therapeutics from a rare disease: weaponizing lipid dysregulation to combat viral infectivity. J Lipid Res 61:972-982.
42. Caly L, Druce JD, Catton MG, Jans DA, Wagstaff KM. 2020. The FDA-approved drug ivermectin inhibits the replication of SARS-CoV-2 in vitro. Antiviral Res 178:104787.
43. https://www.clinicaltrialsregister.eu/ctr-search/search?query=Sars+AND+Ivermectin (accessed November 17, 2020).
44. Yamasmith E, Saleh-arong FA, Avirutnan P, Angkasekwinai N, Mairiang D, Wongsawat E, Tanrumluk S, Fongsri U, Suputtamongkol Y. 2018. Efficacy and safety of Ivermectin against Dengue Infection: A phase III, randomized, double-blind, placebo-controlled trial. The 34th Annual Meeting The Royal College of Physicians of Thailand 'Internal Medicine and One Health'
45. Rogosnitzky M, Okediji P, Koman I. 2020. Cepharanthine: a review of the antiviral potential of a Japanese-approved alopecia drug in COVID-19. Pharmacol Rep doi:10.1007/s43440-020-00132-z.
46. Morales-Ortega A, Bernal-Bello D, Llarena-Barroso C, Frutos-Pérez B, Duarte-Millán M, García de Viedma-García V, Farfán-Sedano AI, Canalejo-Castrillero E, Ruiz-Giardín JM, Ruiz-Ruiz J, San Martín-López JV. 2020. Imatinib for COVID-19: A case report. Clin Immunol 218:108518.
47. Weston S, Coleman CM, Haupt R, Logue J, Matthews K, Li Y, Reyes HM, Weiss SR, Frieman MB. 2020. Broad anti-coronavirus activity of food and drug administration-approved drugs against SARS-CoV-2 in vitro and SARS-CoV in vivo. J Virol 94:e01218-20.
48. Al-Horani RA, Kar S, Aliter KF. 2020. Potential anti-COVID-19 therapeutics that block the early stage of the viral life cycle: Structures, mechanisms, and clinical trials. Int J Mol Sci 21:5224.
49. Schrödinger Release 2020-1; Schrödinger, LLC, New York, NY, 2020.
50. Harder E, Damm W, Maple J, Wu C, Reboul M, Xiang JY, Wang L, Lupyan D, Dahlgren MK, Knight JL, Kaus JW, Cerutti DS, Krilov G, Jorgensen WL, Abel R, Friesner RA. 2016. OPLS3: A force field providing broad coverage of drug-like small molecules and proteins. J Chem Theory Comput 12:281-296.
51. Lan J, Ge J, Yu J, Shan S, Zhou H, Fan S, Zhang Q, Shi X, Wang Q, Zhang L, Wang X. 2020. Structure of the SARS-CoV-2 spike receptor-binding domain bound to the ACE2 receptor. Nature 581:215-220.
52. Waterhouse A, Bertoni M, Bienert S, Studer G, Tauriello G, Gumienny R, Heer FT, de Beer TAP, Rempfer C, Bordoli L, Lepore R, Schwede T. 2018. SWISS-

MODEL: homology modelling of protein structures and complexes. Nucleic Acids Res 46:W296-W303.

53. Case DA, Ben-Shalom IY, Brozell SR, Cerutti DS, Cheatham I, T. E. , Cruzeiro VWD, Darden TA, Duke RE, Ghoreishi D, Gilson MK, Gohlke H, Goetz AW, Greene D, Harris R, Homeyer N, Izadi S, Kovalenko A, Kurtzman T, Lee TS, LeGrand S, Li P, Lin C, Liu J, Luchko T, Luo R, Mermelstein DJ, Merz KM, Miao Y, Monard G, Nguyen C, Nguyen H, Omelyan I, Onufriev A, Pan F, Qi R, Roe DR, Roitberg A, Sagui C, Schott-Verdugo S, Shen J, Simmerling CL, Smith J, Salomon-Ferrer R, Swails J, Walker RC, Wang J, Wei H, Wolf RM, Wu X, Xiao L, et al. 2018. AMBER 2018.

54. Maier JA, Martinez C, Kasavajhala K, Wickstrom L, Hauser KE, Simmerling C. 2015. ff14SB: Improving the accuracy of protein side chain and backbone parameters from ff99SB. J Chem Theory Comput 11:3696-3713.

55. Jorgensen WL, Chandrasekhar J, Madura JD, Impey RW, Klein ML. 1983. Comparison of simple potential functions for simulating liquid water. J Chem Phys 79:926-935.

56. Dolinsky TJ, Nielsen JE, McCammon JA, Baker NA. 2004. PDB2PQR: an automated pipeline for the setup of Poisson-Boltzmann electrostatics calculations. Nucleic Acids Res 32:W665-W667.

57. Ryckaert J-P, Ciccotti G, Berendsen HJC. 1977. Numerical integration fo the cartesian equations of motion of a system with constraints: molecular dynamics of n-alkanes. J Comput Phys 23:327-341.

58. Darden T, York D, Pedersen L. 1993. Particle mesh Ewald: An N·log(N) method for Ewald sums in large systems. J Chem Phys 98:10089-11092.

59. Roe DR, Cheatham TE, 3rd. 2013. PTRAJ and CPPTRAJ: Software for processing and analysis of molecular dynamics trajectory data. J Chem Theory Comput 9:3084-3095.

60. Zeng X, Uyar A, Sui D, Donyapour N, Wu D, Dickson A, Hu J. 2018. Structural insights into lethal contractural syndrome type 3 (LCCS3) caused by a missense mutation of PIP5Kgamma. Biochem J 475:2257-2269.

61. http://research.bmh.manchester.ac.uk/bryce/amber/.

62. Meagher KL, Redman LT, Carlson HA. 2003. Development of polyphosphate parameters for use with the AMBER force field. J Comput Chem 24:1016-1025.

63. Friesner RA, Murphy RB, Repasky MP, Frye LL, Greenwood JR, Halgren TA, Sanschagrin PC, Mainz DT. 2006. Extra precision glide: docking and scoring incorporating a model of hydrophobic enclosure for protein-ligand complexes. J Med Chem 49:6177-6196.

64. Jacobson MP, Pincus DL, Rapp CS, Day TJ, Honig B, Shaw DE, Friesner RA. 2004. A hierarchical approach to all-atom protein loop prediction. Proteins 55:351-367.

65. Corman VM, Landt O, Kaiser M, Molenkamp R, Meijer A, Chu DK, Bleicker T, Brunink S, Schneider J, Schmidt ML, Mulders DG, Haagmans BL, van der Veer B, van den Brink S, Wijsman L, Goderski G, Romette JL, Ellis J, Zambon M, Peiris M, Goossens H, Reusken C, Koopmans MP, Drosten C. 2020. Detection of 2019 novel coronavirus (2019-nCoV) by real-time RT-PCR. Euro Surveill 25:2000045.

66. Bartosch B, Dubuisson J, Cosset FL. 2003. Infectious hepatitis C virus pseudo-particles containing functional E1-E2 envelope protein complexes. J Exp Med 197:633-642.

67. Mingorance L, Friesland M, Coto-Llerena M, Perez-del-Pulgar S, Boix L, Lopez-Oliva JM, Bruix J, Forns X, Gastaminza P. 2014. Selective inhibition of hepatitis C virus infection by hydroxyzine and benztropine. Antimicrob Agents Chemother 58:3451-3460.